Nuclear Science and Techniques (2026) 37:1
https://doi.org/10.1007/s41365-025-01806-0

Crushing evolution in pebble bed based on a novel method: a crushable DEM study

Jian Wang[1,2,3] · Ming-Zhun Lei[2] · Ming-Zong Liu[1] · Qi-Gang Wu[2,4] · Zi-Cong Cai[1] · Kai-Song Wang[1] · Hai-Shun Deng[1]

Received: 14 May 2024 / Revised: 23 July 2024 / Accepted: 6 August 2024 / Published online: 5 December 2025

Abstract
In this paper, a novel method for investigating the particle-crushing behavior of breeding particles in a fusion blanket is proposed. The fractal theory and Weibull distribution are combined to establish a theoretical model, and its validity was verified using a simple impact test. A crushable discrete element method (DEM) framework is built based on the previously established theoretical model. The tensile strength, which considers the fractal theory, size effect, and Weibull variation, was assigned to each generated particle. The assigned strength is then used for crush detection by comparing it with its maximum tensile stress. Mass conservation is ensured by inserting a series of sub-particles whose total mass was equal to the quality loss. Based on the crushable DEM framework, a numerical simulation of the crushing behavior of a pebble bed with hollow cylindrical geometry under a uniaxial compression test was performed. The results of this investigation showed that the particle withstands the external load by contact and sliding at the beginning of the compression process, and the results confirmed that crushing can be considered an important method of resisting the increasing external load. A relatively regular particle arrangement aids in resisting the load and reduces the occurrence of particle crushing. However, a limit exists to the promotion of resistance. When the strain increases beyond this limit, the distribution of the crushing position tends to be isotropic over the entire pebble bed. The theoretical model and crushable DEM framework provide a new method for exploring the pebble bed in a fusion reactor, considering particle crushing.

Keywords Crushing behavior · Granular material · Discrete element method · Pebble bed · Fractal theory

1 Introduction

Granular materials are widely used for tritium breeding and neutron multiplication in the pebble beds of breeding blankets of fusion devices. Understanding the mechanical mechanisms of pebble beds has become crucial in recent years. Numerous studies have been conducted on granular packing characteristics [1–4], mechanical properties of single pebbles [5–7], purge flow characteristics [8–11] and heat-mass transfer [12–14]. Experimental and numerical investigations have been conducted to gain a deeper understanding of pebble beds. However, some studies have proposed that particle crushing is inevitable in the blanket, and the main reasons can be summarized as follows: (1) Granular particles are frequently confined in a random dense packing structure, which means that the surface of a single particle may have multiple contacts with neighbors, resulting in a relatively complicated stress condition. (2) Granular materials are subjected to thermal loads, and the differences in the coefficient of thermal expansion between particles or between particles and structural materials can result in complex loading conditions, leading to particle crushing. (3) Extreme service conditions in fusion reactors require consideration of electromagnetic disturbances and neutron irradiation, which create significant uncertainties in the stress state of

This work was supported by Anhui Provincial Natural Science Foundation (2408085QA030), Natural Science Research Project of Anhui Educational Committee, China (2022AH050825), Medical Special Cultivation Project of Anhui University of Science and Technology (YZ2023H2C008), the Excellent Research and Innovation Team of Anhui Province, China (2022AH010052), the Scientific Research Foundation for High-level Talents of Anhui University of Science and Technology, China (2021yjrc51) and Collaborative Innovation Program of Hefei Science Center, CAS, China (2019HSC-CIP006).

Extended author information available on the last page of the article

the particles. Particle crushing has been observed in some experiments, i.e., ceramic pebbles in the HELICA [15, 16] and EXOTIC [17, 18] facilities exhibit varying degrees of crushing. Particle crushing may affect some key parameters of the fusion blanket, such as the effective thermal conductivity; thus, the possible crushing phenomenon should be considered and a more in-depth study should be conducted on the evolution of the crushing event.

To date, several studies have focused on the crushing behavior of pebble beds. For example, in Ref. [18], a probability analysis model of particle-crushing energy was proposed, and crushing behavior in ceramic pebble beds in a fusion blanket was analyzed. Some researchers [19, 20] considered the critical storage elastic energy as the criterion to determine whether the particles are crushed; after converting the data obtained in the experiment into the equivalent elastic strain energy, Zhao et al. found that the distribution of the equivalent elastic strain energy conformed to the Weibull distribution; thus, an energy-based crushing criterion was applied to a discrete element method (DEM) simulation. Wang et al. [21] established a new method to simulate crushed particles, where the original particle was replaced by several sub-particles, two hemispherical walls of the same diameter as the original particle moved axially in the cylindrical region, and the randomly generated sub-particles were compressed to the location of the last time step before the original particle crushing, keeping the particle at the original point of breakage. Based on the hypothesis of different crushing rates, the evolution law of the mechanical properties was investigated using the DEM. The probabilistic crushing strength of Li_4SiO_4 pebbles was reproduced in DEM simulations using the random sub-ball removal scheme in Ref. [22], and the authors quantitatively analyzed the size-dependent crushing strength and fragment size. Our previous work [23] also established a theoretical model of the crushing behavior description, and the fractal theory and Weibull distribution were combined to describe the size distribution and strength variation. A brief introduction and previous research are included in this paper in Sect. 2.

Currently, only a few studies have been conducted on particle-crushing behavior in fusion blankets, and many reports have been published on particle-crushing behavior in other fields, such as geotechnical engineering [24–27] and chemical engineering [28, 29]. McDowell et al. derived the relationship between the compression rate under a uniaxial compression test (UCT) and the fractal geometry of the crushing and proposed that the premise of using fractal theory is that the particle is assumed continue to crush if the stress continues to increase. Nakata et al. [30] derived a particle-crushing law using a triaxial test based on the statistical distribution of the single-particle-crushing strength, which was determined using single-particle-crushing tests. A limitation of this method is that some assumptions are made when calculating the particle stress for crushing prediction, which lacks experimental evidence, and the stress distribution at the particle level may be highly heterogeneous. The application of scanning electron microscopy (SEM) and computed tomography (CT) for the experimental observation of particle-crushing behavior is of interest [31–34]. High-resolution CT images provided by nanoscale-focused scanners can directly distinguish and quantify the contact between particles, which means that the technology may be used to observe topological evolution in the particle system. However, the limitation of this technology is that CT imaging cannot capture the interaction force between particles, which is essential for understanding crushing behavior.

As demonstrated and discussed above, from theoretical models, experimental studies, and numerical investigations, the evolution of particle crushing in the pebble bed has not been fully studied, and advanced and effective tools to accurately and reasonably model the crushing process are still lacking; thus, the subsequent evolution law cannot be explored. This paper presents a novel method for describing and modeling the pebble bed of a fusion blanket that considers crushable particles in the system. A particle-crushing model that considered the size distribution of fragments, fractal dimension, size effect, and variation in particle strength is derived and demonstrated. Based on the theoretical model, the crushable DEM framework is built and used to explore the evolution of crushing behavior. The paper is organized as follows: The first section has introduced the background and reviewed previous research results. The Section II briefly describes the derivation of the theoretical model; more detailed information can be found in Ref. [23]. Section 3 proposes the crushable DEM framework and calculation process, and Sect. 4 presents a numerical investigation of crushing evolution. The final section presents the conclusions and key findings of the study.

2 Theoretical model

In this paper, a theoretical model for describing crushing behavior is derived by combining fractal theory and the Weibull distribution. During a crushing event, pebbles in a pebble bed break into several sub-parts, and the self-similarity between the sub-parts and the whole can be described using fractal theory. Specifically, the mass of a sub-part within a size of ζL can be expressed as $M(\zeta L) = \zeta^d M(L)$, where L is the size of the original body, and $\zeta < 1$ is the scaling coefficient. Regarding the crushing behavior of the pebble bed, the number of pebbles with radius r, $N(r)$, should follow a fractal distribution:

$$N(r) \propto r^{-D}, \tag{1}$$

where D is the fractal dimension of the crushed pebble bed, and a larger D often indicates a more significant extent of the crushing behavior.

The function $F(r)$ defines the cumulative proportion of particles with radii less than or equal to r. However, because of the dynamic changes caused by crushing events, the particle-size distribution function should also be a function of time τ, denoted by $F(r, \tau)$. The number of particles with radii ranging from r to $r + dr$ is expressed as

$$N_{r\to r+\mathrm{d}r} = k_1 \frac{\partial}{\partial \tau} \frac{\partial F(r,\tau)}{\partial r} \mathrm{d}r \mathrm{d}\,\tau. \tag{2}$$

The proportionality coefficient determined by the material properties is denoted by k_1. The number of particles ranging from r to $r + \mathrm{d}r$ has two sources: First, larger particles with a radius of $a(a > r)$ would break into several pieces, some of which would fall within the interval r to $r + \mathrm{d}r$. This part, denoted as ΔN_1, has a positive effect on $N_{r\to r+\mathrm{d}r}$. Second, particles with a radius of r would break into smaller sub-parts, which negatively influences $N_{r\to r+\mathrm{d}r}$. Therefore, to consider these two factors together, $N_{r\to r+\mathrm{d}r}$ takes the following form:

$$\begin{aligned} k_1 \frac{\partial}{\partial \tau} \frac{\partial F(r,\tau)}{\partial r}\, \mathrm{d}r\, \mathrm{d}\tau = \\ \int_r^{r_{\max}} v(a)\, \mathrm{d}\tau \frac{\partial F(a,\tau)}{\partial a} \frac{\partial \chi(a,r)}{\partial r}\, \mathrm{d}r\, \mathrm{d}a \\ -v(r)\, \mathrm{d}\tau \frac{\partial F(r,\tau)}{\partial r}\, \mathrm{d}r. \end{aligned} \tag{3}$$

In this equation, $v(a)$ denotes the crush rate for particles within the radius r, and $\chi(a, r)$ is the distribution function of larger particles with radius a crushed into sub-particles with radius r. $v(a)$ and $\chi(a, r)$ obey the power laws $v(a) = \alpha r^k$ and $\chi(a, r) = (k/a)^k$. By substituting them into Eq. (3), the solution is obtained as follows:

$$\psi(r,\tau) = \psi(r,0)e^{-\alpha r^k \tau}, \tag{4}$$

where $\psi(r, \tau)$ is the distribution function of particles with radii larger than r, and $\psi(r, \tau) = 1 - F(r, \tau)$. The radius range in the pebble bed of a fusion reactor is typically narrow; thus, $\psi(r, 0)$ can be assumed to be equal 0 for calculation simplification. Eq. (4) can be expressed as

$$\psi(r,\tau) = e^{-\alpha r^k \tau}. \tag{5}$$

Equation (5) can be substituted into the expression of $F(r, \tau)$:

$$D(r,\tau) = 1 - \psi(r,\tau) = 1 - e^{-\alpha r^k \tau}. \tag{6}$$

Combined with the relationship found in previous literature, $\alpha t = {r_c}^{-k}$, Eq. (6) can be rewritten as follows:

$$D(r,\tau) = 1 - e^{\left(-\left(\frac{r}{r_c}\right)^k\right)}. \tag{7}$$

The particle-size distribution function $F(r)$ has the following form:

$$F(r) = \frac{n(r)}{N_t}, \tag{8}$$

where $N(r)$ and $n(r)$ represent the numbers of particles with radii larger and smaller than r, respectively, and the total number of packed pebbles in the bed is denoted by N_t. According to the fractal distribution, the number of particles with a radius larger than r can be expressed in the power-law form: $N(r) \propto r^{-D}$. Here, we substitute its differential form $\mathrm{d}N(r) \propto (-D)r^{-D-1}$ into Eq. (8) and obtained

$$\mathrm{d}F(r) \propto \mathrm{d}n(r) \propto -\mathrm{d}N(r) \propto r^{-D-1}\, \mathrm{d}r. \tag{9}$$

Note that the equations presented above are established based on the number of particles rather than their masses. However, given the large number of particles present in the small pebbles packed in the pebble bed, the mass distribution was used in this study. Specifically, the mass distribution is denoted by $D(r, \tau) = M(r)/M_t = (r/r_c)^k$, where $M(r)$ and M_t represent the mass of particles with radii smaller than r and the total particle mass, respectively. The differential form of the mass distribution can be expressed as

$$\mathrm{d}M(r) = M_t\, \mathrm{d}D(r,\tau) = \frac{4}{3}\pi\rho r^3\, \mathrm{d}n(r), \tag{10}$$

where ρ is the density of the pebble material. Taking the above equations together, the differential form of $F(r, \tau)$ is $\mathrm{d}D(r, \tau) \propto r^{2-D}\, \mathrm{d}r$. Thus, $F(r, \tau)$ can be obtained by integrating its differential form:

$$D(r,\tau) = \int_0^r r^{2-D}\, \mathrm{d}r = Ar^{3-D}. \tag{11}$$

By comparing the initial $(D(r, \tau) = M(r)/M_t = (r/r_c)^k \propto r^k)$ and final forms $(D(r, \tau) = Ar^{3-D})$ of $F(r, \tau)$, the relationship between the fractal dimension and the parameter k can be derived as

$$k = 3 - D. \tag{12}$$

When considering the crushing strength of pebbles in a packed bed, the size effect must be considered, as the pebble bed in a fusion reactor may not have a mono-sized distribution because of the initial polydisperse arrangement (e.g., the beryllium bed used for neutron multiplication) or the crushing behavior of pebbles. The crushing strength is typically determined using uniaxial compression tests on several particles and can be calculated as $\sigma_c = F_c/S_c$, where F_c and S_c are the crushing loads obtained in the compression tests and nominal contact area between the particle and plate.

For spherical pebbles used in a fusion reactor, S_c must follow $S_c \propto r^2$.

In addition to the crushing strength, the inherent crushing strength σ_e is introduced here, which is determined solely by the material properties and is defined as $\sigma_e = F_c/S_a$, where S_a denotes the actual contact area. According to fractal theory, the contact area between the particle and compression plate can be considered a transformation process from a higher dimension (3D) to a lower dimension (2D), resulting in the reduction in the particle's dimension by 1. Therefore, for a crushed pebble bed with an original fractal dimension of D, the contact area can be expressed as

$$S_a \propto r^{D-1}. \tag{13}$$

Taken together, we can obtain the relationship between the crushing strength and fractal dimension: $\sigma_c = \sigma_e r^{D-3}$. For clarity, its logarithmic form is used:

$$\log \sigma_c = (D-3)\log r + f(\sigma_e). \tag{14}$$

The crushing strength frequently demonstrates significant variations owing to the existence of initial defects and cracks. The Weibull distribution has been widely used to predict survival probability when particles are subjected to a specific external load. The Weibull distribution can be expressed as

$$P_n(\sigma, n) = \exp\left[-n\left(\frac{\sigma}{\sigma_0}\right)^m\right], \tag{15}$$

where σ_0 is the characteristic stress, and m denotes the Weibull modulus. Often, the parameter n has the following form: $n = (\frac{r}{r_0})^3$. However, in this paper, to implement the fractal theory in the theoretical model, we rewrite n as $n = (\frac{r}{r_0})^D$ [23] and Eq. (15) as

$$P_n(\sigma, r) = \exp\left[-\left(\frac{r}{r_0}\right)^D\left(\frac{\sigma}{\sigma_0}\right)^m\right]. \tag{16}$$

To determine the mathematical correlation between m and D, which are the two main parameters in the Weibull and fractal theories, and for the probability illustrated in the above equations to be constant, i.e., $\left[-\left(\frac{r}{r_0}\right)^D\left(\frac{\sigma}{\sigma_0}\right)^m\right] = C$, we can obtain the following relationship:

$$m = D/(3-D). \tag{17}$$

A series of impact tests was conducted to verify the validity of the theoretical model established in this paper. The test apparatus, as shown in Fig. 1, consisted of a cylindrical container mounted on a base, a drop hammer weighing 286 g, screens (0.0625 − 5 mm), a high-precision electronic scale, and glass particles. Spherical glass particles with a radius of r =2.5 mm (specific gravity: 2.4 − 2.6 g/cm^3) were used to form a packed bed. Note that glass particles were used owing to their widespread use in previous studies. Different particles may have significant differences in the physical properties and mechanical behavior. However, the impact test aimed to simulate the key characteristics, crushing behavior, and evolution of pebble accumulation; the influence of material performance differences was not significant. The number of bed layers n, impact time i, and drop height h were varied. After each impact test, the particles were sieved manually to obtain the mass distribution within each range. The cumulative distribution was plotted in a double logarithmic coordinate system, and the fractal dimension of particle crushing

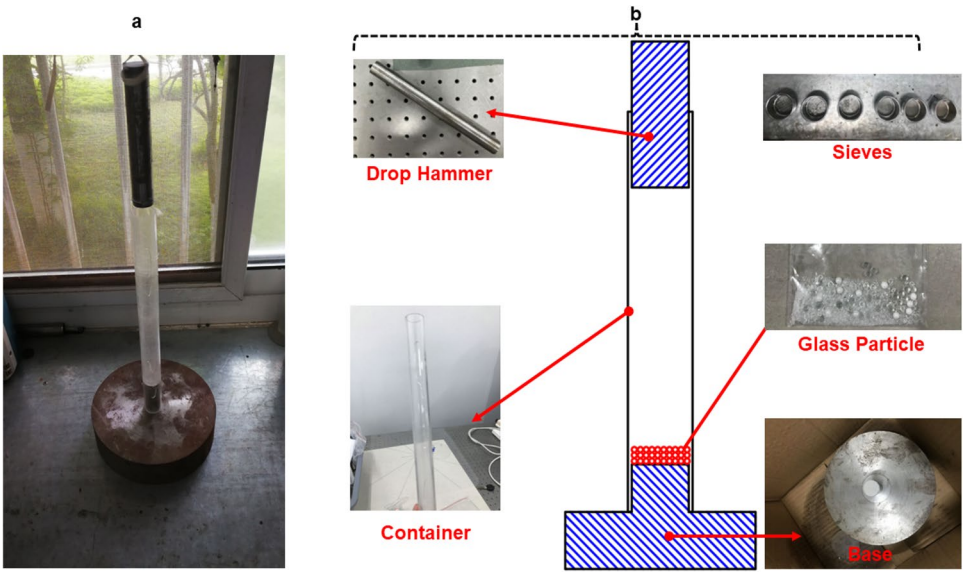

Fig. 1 (Color online) Test apparatus used to validate the theoretical model

was calculated using the slope k of the fitted straight lines according to Eq. (12). Three replicates were performed for each group to minimize test errors.

Single-layer ($n = 1$) and two-layer ($n = 2$) pebble beds with 12 and 24 particles, respectively, were formed. The impact times were varied in the ranges of 16–20 ($n = 1, h =$ 15.5 cm), 5–11 ($n = 1, h =$20.5 cm), 26–28 ($n = 2, h =$ 35 cm), and 17–21 ($n = 2, h =$40.5 cm). The experimental results are presented in Fig. 2. Each data point in the figure represents the mean of three replicates and is denoted by $D_{ni}(h)$, where n and i are the number of bed layers and the impact time, respectively. The subscripts n and i represent the exact values. The letter h in parentheses indicates the hammer drop height during the test. The y-axis denotes the logarithm of the cumulative distribution ϕ_r, and the x-axis is the logarithm of the particle radius r. The sub-figure in each plot shows the relationship between the impact energy of the unit mass particles E_m and the fractal dimension $D_{ni}(h)$. E_m is calculated as $E_m = E/m_p = imgh/m_p$ (J/kg), where m and m_p denote the weight of drop hammer and particles, respectively.

The experimental results shown in Fig. 2 demonstrated highly significant linear trends in all the test cases. The fractal dimension of the particle-crushing behavior changed with the impact time, number of bed layers, and drop height. Specifically, the fractal dimension increased with the impact time, indicating an increase in the extent of crushing. However, with an increase in the impact energy, the fractal dimension, which can be considered a measure of the degree of crushing, reached a limit beyond which the pebbles in the packed bed could not be crushed any further. This phenomenon corresponded with physical practice.

Another aspect of concern is the evolution rate of crushing behavior in a packed bed. For the single-layer packed bed results shown in Fig. 2a and b, the impacts required to achieve the final state were five and seven at $h =$15.5 cm and $h =$20 cm, respectively. For the two-layer bed, the required impact times were 3 and 5, respectively. These results

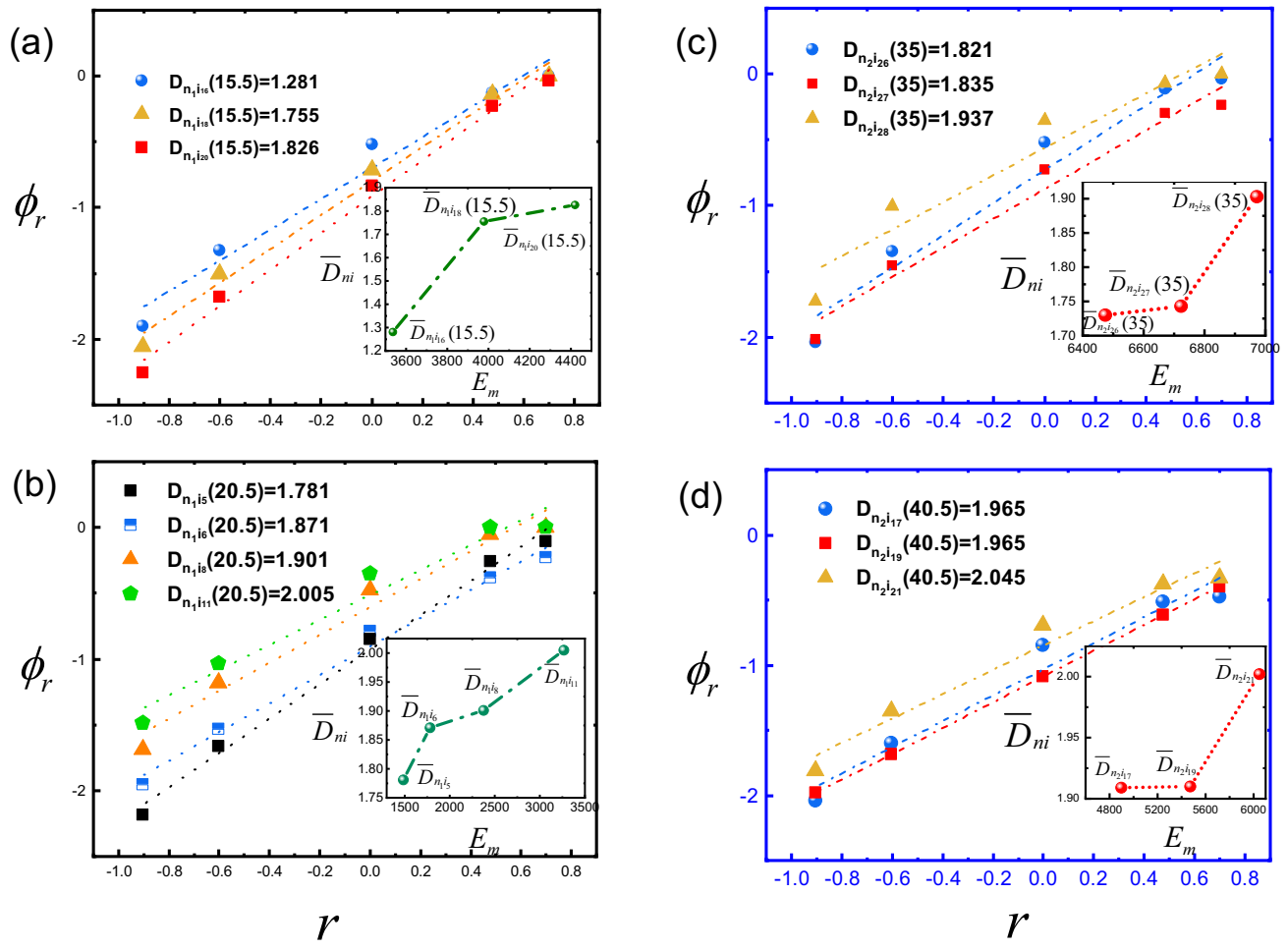

Fig. 2 (Color online) Experimental results in the impact test. **a**, **b**: Fractal dimension D under different impact times i for single-layer packed bed ($n = 1$) **a**: $h = 15.5$ cm; **b**:$h = 20.5$ cm; **c**, **d**: Fractal dimension D under different impact times i for two-layer packed bed ($n = 2$) **c**:$h = 35$ cm; **d**:$h = 40.5$ cm

suggest that the rate of crushing evolution changes more rapidly in a two-layer bed than in a single-layer bed. In contrast, the opposite was true for the amount of change in the fractal dimension. The test results showed that ΔD was 0.545 (h =15.5 cm), 0.2247 (h =20.5 cm) for single-layer beds, and 0.116 (h =35 cm), 0.08 (h =45.5 cm) for two-layer beds. These results can be explained by the fact that the contact and topology are more stable in a two-layer bed because the pebbles can resist external loading through pebble–pebble and pebble–wall contacts. The network force chain generated in a two-layer bed can withstand impact loading in the axial direction. For single-layer beds, axial force chains cannot be used to resist loading, resulting in a more dramatic change in the extent of crushing.

3 Crushable DEM framework

3.1 Discrete element method

In this paper, a numerical method based on the established theoretical model within the DEM framework is demonstrated and used to study crushing behavior evolution in the pebble bed of a helium-cooled ceramic breeder (HCCB) blanket. Cundall and Strack proposed the DEM, and its model involves two stages: (1) The interaction force is calculated performed based on the provided particle positions and mechanical models when a pair of particles interpenetrate each other; (2) the acceleration of the particles is then determined using the force obtained in the last step and Newton's second law, and the new position of the particle is calculated using time-stepping integration.

Newton's law is expressed as follows:

$$\sum F_i = m_i v_i, \sum M_i = I_i \omega_i, \tag{18}$$

where m and I denote the mass and moment of inertia, respectively. v and ω are the translational and angular velocities, respectively. F_i and M_i represent the force and relevant torque applied to the particle, respectively. The force applied to the particle body consists of several parts, which can be expressed as $F_i = F_\mathrm{b} + F_\mathrm{c} + F_\mathrm{external}$, where F_b, F_c, and F_external represent the body, contact, and external forces, respectively. The contact force F_c can be divided into normal and tangential forces, denoted as F_n and F_t, respectively. The normal and tangential contact forces are functions of the overlaps (δ_n or δ_t) and relative velocities (v_n or v_t) between the contact pairs. The detailed calculation methods for F_n and F_t are given as

$$F_\mathrm{n} = (-4/3)E^* \sqrt{(R^* \delta_\mathrm{n})} - 2\sqrt{5/6}\beta \sqrt{(S_\mathrm{n} m^*)} v_\mathrm{n}, \tag{19}$$

$$F_\mathrm{t} = -8G^* \sqrt{(R^* \delta_\mathrm{n})} \delta_\mathrm{t} - 2\sqrt{5/6}\beta \sqrt{(S_\mathrm{t} m^*)} v_\mathrm{t}, \tag{20}$$

where E^* and R^* denote the equivalent modulus and radius and can be calculated as $\frac{1}{E^*} = \frac{1-\sigma_1^2}{E_1} + \frac{1-\sigma_2^2}{E_2}$ and $\frac{1}{R^*} = \frac{1}{R_1} + \frac{1}{R_2}$, respectively, where E, σ, and R are the particles' Young's modulus, Poisson's ratio, and radius, respectively. The overlap in the normal and tangential directions is a critical variable during the force calculation. The normal overlap δ_n can be easily determined using $\delta_\mathrm{n} = R_1 + R_2 - d_{12}$, where R_1, R_2, and d_{12} represent the radii of particles 1 and 2 and the distance between the two particle centers, respectively. The tangential overlap δ_t requires an integral of the tangential velocity $\delta_\mathrm{t} = \int_{\Delta t} v_\mathrm{t} \mathrm{d}t$. The normal stiffness S_n and tangential stiffness S_t in Eq. (20) are given as $S_\mathrm{n} = 2E^* \sqrt{R^* \delta_\mathrm{n}}$, $S_\mathrm{t} = 8\,G^* \sqrt{R^* \delta_\mathrm{n}}$, where the equivalent shear modulus $G^* = \frac{2-\sigma_1^2}{G_1} + \frac{2-\sigma_2^2}{G_2}$, G represents shear modulus of particles: $G = E/(2+2\mu)$ (μ: coefficient of friction). The damping effect can be introduced by setting an appropriate coefficient of restitution e, which can be considered a function of e: $\beta = \ln e / \sqrt{\ln^2 e + \pi^2}$. Coulomb's friction law is used to determine the occurrence of sliding between particles: $F_\mathrm{t} = -\mu |F_\mathrm{n}| \frac{\delta_\mathrm{t}}{\delta_\mathrm{n}}$.

3.2 Stress and strength in the DEM

Generally, a UCT can measure the crushing strength of a single particle. However, as a granular assembly, the crushing strength of pebbles in a pebble bed may differ significantly from that of a UCT because the pebble stress is affected by the multi-contact scenario, which results in a much more comprehensive stress condition. Extensive research has proved that the results obtained in DEM simulations, where the tensile strength of particles was used as the breakage criterion, agree closely with experimental data. Therefore, in this study, tensile strength was selected to control the occurrence of particle crushing. To connect the contact force in mesoscopic with the stress level macroscopically, we use the following equation:

$$\sigma_{mn} = \frac{\sum_{i=1}^{Z} l_m^i f_n^i}{V_\mathrm{s}}, \tag{21}$$

where V_s and Z denote the particle volume and coordination number, respectively. l_m^i denotes the m-th component of the unit normal vector of the i-th contact. f_n^i denotes the n-th component of the i-th contact force vector. For a 3D simulation, the primary and secondary stresses of a particle can be calculated as follows:

$$\sigma_1 = \frac{\sigma_{11} + \sigma_{33}}{2} + \sqrt{(\frac{\sigma_{11} - \sigma_{33}}{2})^2 + \sigma_{13}\sigma_{31}}, \tag{22}$$

$$\sigma_3 = \frac{\sigma_{11} + \sigma_{33}}{2} - \sqrt{\left(\frac{\sigma_{11} - \sigma_{33}}{2}\right)^2 + \sigma_{13}\sigma_{31}}. \quad (23)$$

The maximum tensile stress should be perpendicular to the direction of the first principal stress and is given as

$$\sigma_{t,\max} = (\sigma_1 - 3\sigma_3)/2. \quad (24)$$

Thus, $\sigma_{t,\max}$ of each generated particle is calculated at every timestep, and $\sigma_{t,\max}$ is compared with the tensile strength of the particle, whose calculation and assignment processes are discussed below.

The established theoretical crushing model suggests that the crushing strength can be calculated using Eq. (16), which has been modified by considering the fractal theory and Weibull distribution. The variation in the particle-crushing strength is first discussed by considering a mono-sized pebble bed, where the size effect of the crushing strength could be neglected. r in Eq. (16) can be considered a constant equal to the reference radius r_0, and Eq. (16) takes a new form:

$$P_n(\sigma, n) = \exp\left[-\left(\frac{\sigma}{\sigma_0}\right)^m\right]. \quad (25)$$

To obtain the probability distribution of the particle-crushing strength, we must derive Eq. (25).

$$p_n(\sigma, n) = \frac{m}{\sigma_0}\left(\frac{\sigma}{\sigma_0}\right)^{m-1} \exp\left[-\left(\frac{\sigma}{\sigma_0}\right)^m\right]. \quad (26)$$

The size effect of the crushing strength is reconsidered by modifying the above equation based on fractal theory:

$$p_n(\sigma, n) = \frac{m}{\sigma_0}\left(\frac{\sigma}{\sigma_0}\right)^{m-1} \exp\left[-\left(\frac{\sigma}{\sigma_0}\right)^m\right]\left(\frac{r}{r_0}\right)^D. \quad (27)$$

The tensile strength of a particle of radius r is calculated using Eq. (27). The tensile strength is assigned to each particle when the particle is generated. From a single-particle perspective, the given tensile strength is random owing to the randomness of the Weibull distribution, whereas from a pebble bed perspective, the assigned tensile strength of all the particles obeys the Weibull distribution, which is consistent with the characteristics of the strength variation caused by randomly distributed initial cracks and defects. The maximum tensile stress on each particle is updated using Eq. (24) at every timestep and compared with its tensile strength, which is calculated using Eq. (27). The particle breaks when $\sigma_{t,\max} > p_n(\sigma, r)$.

3.3 Crushable DEM framework

A detailed schematic of the crushable DEM framework is presented in Fig. 3. Local stress mutations frequently exist when the crushing of particles occurs because the particles are broken into several pieces, and the spatial distribution of solid particles experiences a dramatic change. We adopt the radius reduction method to reproduce the local stress mutations used in our previous study. The particle determined to be crushed would experience a radius reduction from r to $0.5r$. However, the mass of the pebble bed decreases as the radius of the crushed particles decreases; thus, system mass loss occurs and can be conserved by injecting sub-particles into the pebble bed. The mass loss introduced by a single particle is calculated as

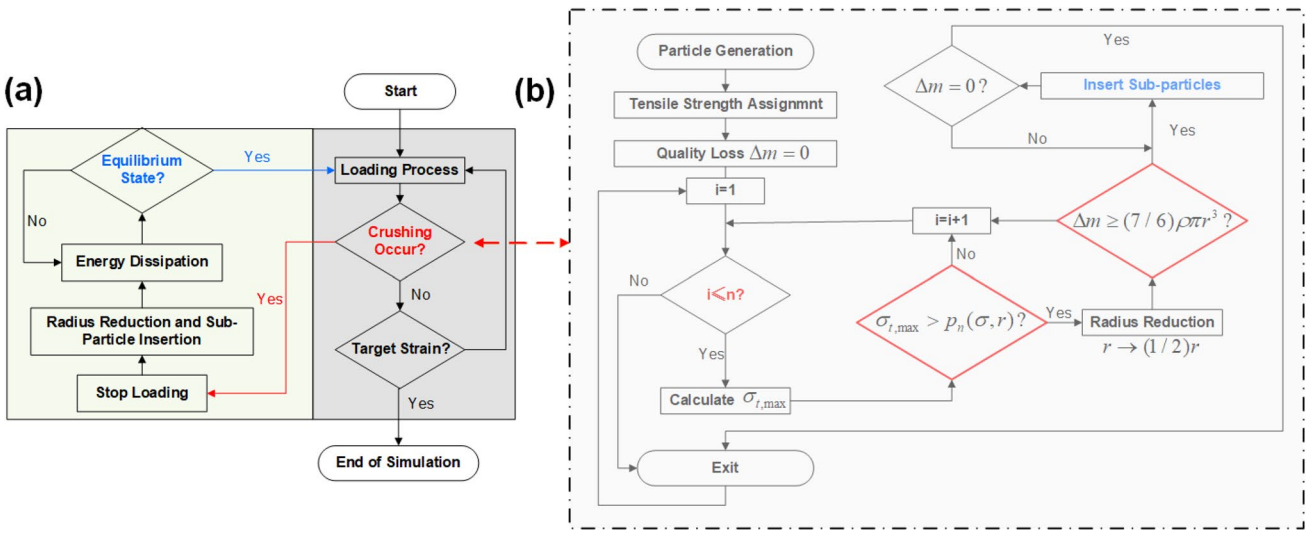

Fig. 3 (Color online) Framework of crushable DEM

$\Delta m = 4\left(\pi r^3\rho - \pi\left(\frac{R}{2}\right)^3\rho\right)/3 = 7\pi\rho r^3/6$. The total mass of the pebble bed was monitored during the simulation, and several sub-particles were randomly inserted into the pebble bed when the mass loss of the pebble bed system was greater than $7\pi\rho r^3/6$. The feasibility of this sub-particle insertion approach is validated in Ref. [35].

We now examine the sub-particles injected into the system. Using the established theoretical model, the size distribution of the particle fragments was assumed and proven to obey the fractal distribution. The integral interval in Eq. (11) was changed from $0 \to r$ to $r_1 \to r_2$, and the proportion of the mass of particles with radii between r_1 and r_2 can be obtained as follows:

$$\int_{r_1}^{r_2} r^{2-D}\mathrm{d}r = (3-D)(r_2^{3-D} - r_1^{3-D}). \tag{28}$$

Granular materials lithium orthosilicate (OSi) and lithium metatitanate (LMT) are commonly used in fusion blankets for tritium breeding. Consequently, we selected to simulate OSi pebbles (Li_4SiO_4 pebbles) in the crushable DEM case. The Weibull modulus m and characteristic stress σ_0 for the Li_4SiO_4 pebbles with a radius of 0.5 mm were obtained from experiments conducted by other researchers: σ_0 =30.2 MPa and $m = 3.97$. Using Eq. (17), we calculated the fractal dimension of the Li_4SiO_4 pebble as $D = 3m/(m+1) = (3\times 3.97)/(3.97+1) \doteq 2.396$. Consequently, we can rewrite Eq. (28) as follows:

$$M_{r_1\to r_2} = 0.604(r_2^{0.604} - r_1^{0.604}) \propto r_2^{0.604} - r_1^{0.604}. \tag{29}$$

This equation relates to the change in mass between the two radii, r_1 and r_2, of the OSi pebbles.

For a lower computing cost, the radius range of inserted sub-particle was limited to $0.08 - 0.24$ mm, and the sub-particle size followed the fractal distribution with fractal dimension $D = 2.396$. The size distributions of r, calculated using Eq. (29), are listed in Table 1.

Table 1 Mass and quantity percentage of inserted sub-particles

Radius, r (mm)	0.08–0.12	0.12–0.16	0.16–0.20	0.20–0.24
Mass percentage (%)	29.47	25.74	23.29	21.50
Quantity percentage (%)	65.69	20.91	8.90	4.50

4 Crushable DEM simulation of UCT on the pebble bed in a fusion blanket

4.1 Numerical experiment setup

The crushable DEM framework was implemented in LIGGGHTS-PUBLIC, which is an open-source DEM particle simulation software based on LAMMPS. An annular cylinder container model with an outer diameter d_{out} =57 mm, inner diameter d_{in} =17 mm, and height H =156 mm [36] was constructed and imported into LIGGGHTS as an .stl file to hold OSi particles. Li_4SiO_4 pebbles were generated from an insertion face located at the top of the container and were allowed to fall under gravity. Ultimately, 423736 Li_4SiO_4 pebbles were packed into a container. The total kinetic energy of the system k_n was closely monitored during the packing and rearrangement processes, and the system was considered to be in equilibrium when $k_n < 1\times 10^{-10}$ J. When equilibrium was reached, a compression plate was used to compress the pebble bed at a constant velocity of 0.1 mm/s in the negative z-direction. The compression process ended when a target bed strain of 0.35% was reached, where the bed strain was defined as the ratio of the change in bed height to the initial bed height: $\varepsilon = \Delta H/H_i$. Table 2 lists the details of the DEM parameters used in the simulations. As the pebble bed consisted of spherical pebbles made of a high Young's modulus material and rolling friction is typically used to account for particle shape and interparticle contact, the rolling friction model was omitted in this study to reduce computational costs.

4.2 Results and discussion

Figure 4a–g depicts the evolution of the number of crushed particles (denoted as ξ in the figures) during the loading

Table 2 Main parameters in the crushable DEM simulation (LIGGGHTS−3.80)

Parameter	Value
Diameter for original particle, d_1 (mm)	1
Diameters for crushed particle, d_2 (mm)	0.5
Diameters for sub-particle, d_s (mm)	see Table 1
Density, ρ_p (kg/m^3)	2323
Young's modulus for particle, E_p (GPa)	90
Young's modulus for wall, E_w (GPa)	200
Poisson's ratio for particle, ν_p	0.24
Poisson's ratio for wall, ν_w	0.23
Coefficient of restitution, e	0.1
Coefficient of friction, μ	0.3
Compression rate, V (mm/s)	0.1

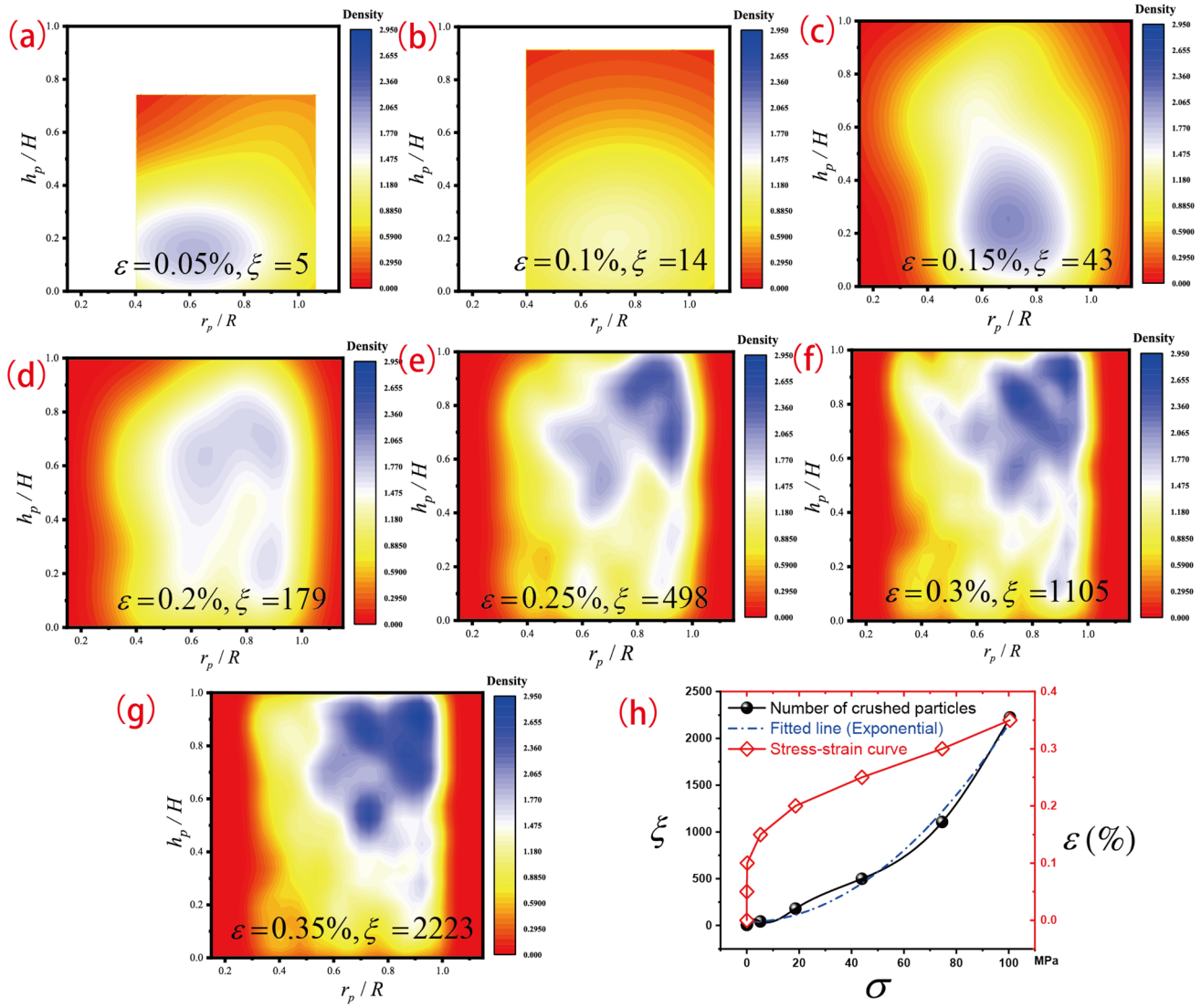

Fig. 4 (Color online) Evolution of particle-crushing behavior. **a**–**g** *Hot zone* distribution evolution under the UCT. (**h**) Stress–strain relationship and change trend of the crushed particle number with stress

phase, with the radial (r_p) and axial (h_p) positions normalized by the cylindrical radius (R) and height (H). As the bed strain ε increased from 0% to 0.35%, the value of ξ also increased dramatically from 5 to 2223 as a direct result of the larger stress applied to the pebbles because of the more significant bed strain. Typically, granular assemblies resist mechanical loading through a rearrangement process that occurs within the spatial topology of the system. However, there are limitations to this resistance ability, beyond which the particle-crushing process must be employed to enable external load sharing throughout the system.

The distributed densities of the crushed particles for each case are plotted in Fig. 4a–g, which highlights areas with relatively high densities as *hot zones*, which appear darker in color. The changing trend of the *hot zones* could be analyzed in both the horizontal (x) and vertical (y) directions. The *hot zone* was observed to move toward the right side with increasing bed strain along the x direction, indicating that the primary crushing events mostly occurred at the center of the pebble bed. As the compression loading increased, more crush events occurred near the container wall, highlighting the wall effect of the crush event locations, as well as the packing structure. The stress condition near the container wall became increasingly complex with an increase in compressive loading, resulting in a relatively looser packing structure and a larger gradient of the stress field compared to the central area, potentially resulting in a stress state mutation in the near-wall region. Pebbles have a coping mechanism called crushing to solve stress state mutations. Therefore, we can conclude that the spatial topology

influences the occurrence of crushing events in the pebble bed. A crushing wall effect similar to that of the packing factor was observed during the loading phase, in which the stress field changed more dramatically. The crushing of particles acted as a protective mechanism to prevent the failure of the granular material.

Regarding the changing tendency of the *hot zone* along the axial direction of the pebble bed, the figure shows that the *hot zone* moved upward with increased external compression in the normalized coordinate system. This suggests that when the bed strain increased, the location of particle crushing shifted to the top of the bed. During the initial compression stage, the particles located at the bottom of the pebble bed were more susceptible to crushing because of the larger loading resulting from the gravity of the upper particles. Specifically, the gravitational force played a significant role in the particle-crushing behavior. As the bed strain increased, the bed stress also increased, whereas the gravitational field remained constant, resulting in a decrease in the share of gravity in the total particle loading and a subsequent reduction in the impact of gravity. The granular system transformed into a state dominated by mechanical loading. More crushing events occurred near the contact area between the plate and pebble bed, indicating that the stress conditions were much more complex than those at other positions. The changing trend of the *hot zone* in the axial direction further corresponded with the conclusions drawn in the previous section. The internal spatial topology of the pebble bed significantly influences the occurrence of particle crushing. Along the axial direction, the presence of the compression plate led to an increased degree of randomness in particle stacking, and the spatial topology structure became increasingly unpredictable in regions closer to the plate. Overall, in the axial direction, the particles could resist gradually increasing external mechanical loads by undergoing particle crushing. The crushing of particles in the upper layers also protects the integrity of the lower layers to some extent, preventing them from being damaged. This protective effect can effectively prevent a significant reduction in the tritium breeding performance of a blanket subjected to unexpectedly large axial loads.

The stress–strain relationship and the change trend of the number of crushed particles with stress are plotted in Fig. 4h. The power-law relationship between the number of crushed particles and stress in the bed can be observed from the graph, which is somewhat analogous to the relationship between stress and strain. As the strain on the pebble bed continued to increase, the axial load on the granular material also increased, and the generated stress rapidly increased with increasing magnitude and speed owing to the gradual collapse of the internal mechanism that initially resisted the external loads. Relying solely on measures such as friction, shear, compression, small deformation of particles, and spatial topological adjustment cannot ensure the stability of the bed structure under a gradually increasing external load. Therefore, the pebble bed must rely on the particle-crushing mechanism to resist the load, leading to an accelerated increase in the number of particle fragmentation events with increasing stress, which is consistent with the conclusions obtained in the previous section.

To distinguish the spatial distribution of crushing events in the pebble bed more clearly, as shown in Fig. 5, we divided the bed into five layers radially and enumerated the number of crushed particles per layer separately. The entire pebble bed, except for the central portion with a diameter of 17 mm, was evenly divided radially into five layers, each with a mirrored gap of 8 mm (Δd =8 mm). The numbers of crushed particles in each layer are shown in Fig. 6. The abscissa and ordinate denote the normalized number of crushed particles and radial position, respectively, i.e., the absolute number of crushed particles N_i, which are indicated by the red numbers in Fig. 6, was normalized by the corresponding layer volume V_i, and the actual radial coordination r was normalized by the radius of the pebble bed R Thus, the normalized N_i/V_i could be regarded as a function of the radial position r/R. In Fig. 6, from the observation of the evolution of crush events during the compression process, we found that the crush event distribution was not uniform in each radial layer when the bed strain was small, and the particle-crushing phenomenon was most acute in the middle of the radial inner and outer walls of the bed. With increasing bed strain ε, the crushed particles were primarily distributed in the outer part of the bed, which may have been due to the regularity of the particle arrangement, which weakened when the radial distance was large, resulting in a more complex stress scenario. The particles near the inner wall maintained a lower overall crushing level at a lower strain, which significantly benefited from the more regular

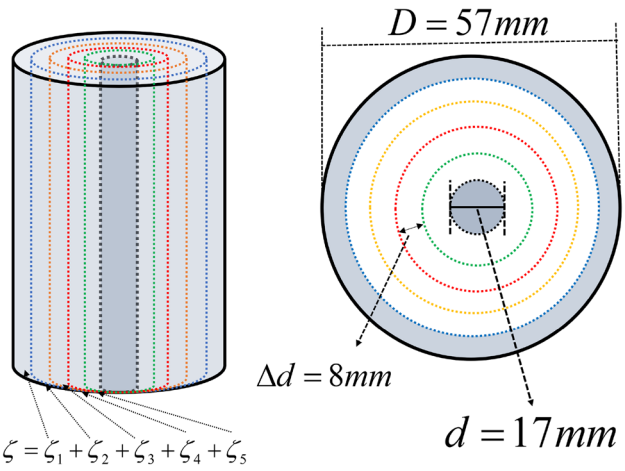

Fig. 5 Schematical view of layer distribution in the radial direction

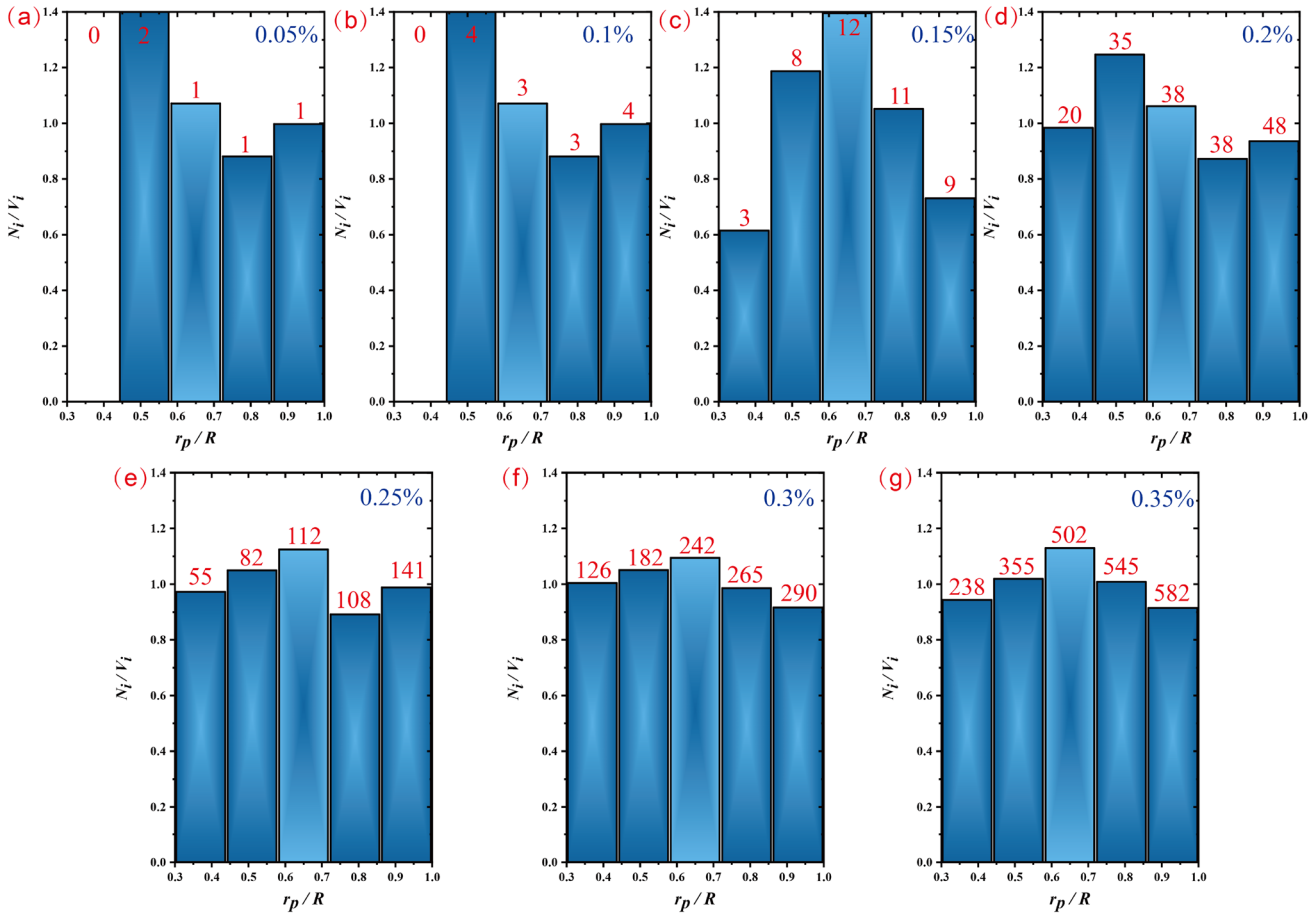

Fig. 6 (Color online) Number of crushed particles in each radial layer; the absolute number of crushed particles are indicated by red numbers

particle arrangement. However, the spatial nonuniformity of particle crushing gradually diminished as the external load increased. When the strain rate of the bed reached 0.3% under conditions of substantial external load, the arrangement and topological structure of the particles had a minimal influence on the distribution of the particle-crushing locations. At this point, the crushing of particles was primarily governed by the external load.

5 Conclusion

In this paper, we propose a novel method for investigating the crushing behavior of breeding particles in a fusion blanket. The fractal theory and Weibull distribution were combined to establish a theoretical model, and its validity was verified using a simple impact test. Subsequently, a crushable DEM framework is proposed based on a theoretical model that incorporates the DEM. The tensile strength, which considers the fractal theory, size effect, and Weibull distribution, was assigned to each generated particle, and the assigned strength was then used for crush detection by comparison with its maximum tensile stress. Mass conservation was ensured by inserting a series of sub-particles whose total mass was equal to the quality loss. Based on the crushable DEM framework, a numerical simulation of the crushing behavior of a pebble bed with a hollow cylindrical geometry under uniaxial compression test was performed. The results of this investigation showed that the particle withstands the external load by contact and sliding at the beginning of the compression process, and the results confirmed that crushing can be considered an important means of resisting the increasing external load. A relatively regular particle arrangement aids in resisting the load and reduces the occurrence of particle crushing. However, a limit to the promotion of resistance exists. When the strain increases beyond this limit, the distribution of the crushing position tends to be isotropic over the entire pebble bed.

Overall, this study established a theoretical model to investigate particle-crushing behavior in a fusion blanket and provided a crushable DEM framework for numerical simulations. A limitation of this study was that the effect of a special multiphysics coupling field in a fusion reactor was not included or considered in the crushing model because of

the lack of experimental data. Further research is required to better understand the particle-crushing behavior in fusion blankets.

Author contributions All authors contributed to the study conception and design. Material preparation, data collection and analysis were performed by Jian Wang, Ming-Zong Liu and Ming-Zhun Lei. The first draft of the manuscript was written by Jian Wang, and all authors commented on previous versions of the manuscript. All authors read and approved the final manuscript.

Data availability The data that support the findings of this study are openly available in Science Data Bank at https://cstr.cn/31253.11.sciencedb.28381 and https://www.doi.org/10.57760/sciencedb.28381.

Declarations

Conflict of interest The authors declare that they have no Conflict of interest.

References

1. J. Wang, M. Lei, H. Yang et al., Study on the packing characteristics of a special "J'' shape ceramic packed pebble bed based on discrete element modeling. Powder Technol. **379**, 362–372 (2021). https://doi.org/10.1016/j.powtec.2020.10.076
2. Q. Wu, M. Lei, J. Wang et al., Packing characteristics of pebble beds for fusion reactors under different friction coefficients. Fusion Eng. Des. **176**, 113051 (2022). https://doi.org/10.1016/j.fusengdes.2022.113051
3. W. Xi, Q. Wu, M. Lei et al., Numerically investigation of the neutron irradiation swelling on the mechanical and structural evolution of beryllium pebble bed. Fusion Eng. Des. **195**, 113966 (2023). https://doi.org/10.1016/j.fusengdes.2023.113966
4. D. Sohn, Y. Lee, M.Y. Ahn et al., Numerical prediction of packing behavior and thermal conductivity of pebble beds according to pebble size distributions and friction coefficients. Fusion Eng. Des. **137**, 182–190 (2018). https://doi.org/10.1016/j.fusengdes.2018.09.012
5. G. Piazza, J. Reimann, E. Günther et al., Behaviour of ceramic breeder materials in long time annealing experiments. Fusion Eng. Des. **58**, 653–659 (2001). https://doi.org/10.1016/S0920-3796(01)00517-8
6. M. Lei, Q. Wu, S. Xu et al., Crushing behaviour of Li_4SiO_4 and Li_2TiO_3 ceramic particles. Nucl. Mat. Energy **31**, 101188 (2022). https://doi.org/10.1016/j.nme.2022.101188
7. J. Van Der Laan, H. Kawamura, N. Roux et al., Ceramic breeder research and development: progress and focus. J. Nucl. Mater. **283**, 99–109 (2000). https://doi.org/10.1016/S0022-3115(00)00352-4
8. Z. Wu, Y. Wu, C. Wang et al., Experimental and numerical study on helium flow characteristics in randomly packed pebble bed. Ann. Nucl. Energy **128**, 268–277 (2019). https://doi.org/10.1016/j.anucene.2019.01.016
9. C. Sedani, M. Panchal, P. Chaudhuri, Simulation and experimental analysis of purge gas flow characteristic for pebble bed. Fusion Eng. Des. **172**, 112778 (2021). https://doi.org/10.1016/j.fusengdes.2021.112778
10. S. Bu, J. Yang, Q. Dong et al., Experimental study of flow transitions in structured packed beds of spheres with electrochemical technique. Exp. Therm. Fluid Sci. **60**, 106–114 (2015). https://doi.org/10.1016/j.expthermflusci.2014.09.001
11. X. Jia, N. Gui, X. Yang et al., Experimental study of flow field characteristics on bed configurations in the pebble bed reactor. Ann. Nucl. Energy **102**, 1–10 (2017). https://doi.org/10.1016/j.anucene.2016.12.009
12. L. Liu, J. Deng, D. Zhang et al., Review of the experimental research on the thermal-hydraulic characteristics in the pebble bed nuclear reactor core and fusion breeder blankets. Int. J. Energ. Res. **45**, 11352–11383 (2021). https://doi.org/10.1002/er.5378
13. H. Chen, S. Wang, C. Jin et al., Theoretical and experimental study on effective thermal conductivity of pebble bed for fusion blanket. Fusion Eng. Des. **124**, 792–796 (2017). https://doi.org/10.1016/j.fusengdes.2017.03.169
14. S. Yu, Z. Zhang, C. Peng et al., Rapid analysis of packed pebble beds for thermal-hydraulic characteristics via reduced order models. Chem. Eng. Sci. **280**, 119029 (2023). https://doi.org/10.1016/j.ces.2023.119029
15. G. Dell'Orco, A. Ancona, A. DiMaio et al., Thermo-mechanical testing of Li-ceramic for the helium cooled pebble bed (HCPB) breeding blanket. J. Nucl. Mater. **329**, 1305–1308 (2004). https://doi.org/10.1016/j.jnucmat.2004.04.225
16. Y. Gan, M. Kamlah, Thermo-mechanical analyses of helica and hexcaliber mock-ups. J. Nucl. Mater. **386**, 1060–1064 (2009). https://doi.org/10.1016/j.jnucmat.2004.04.225
17. A. Ying, M. Akiba, L. Boccaccini et al., Status and perspective of the R&D on ceramic breeder materials for testing in ITER. J. Nucl. Mater. **367**, 1281–1286 (2007). https://doi.org/10.1016/j.jnucmat.2007.03.240
18. Y. Gan, M. Kamlah, H. Riesch-Oppermann et al., Crush probability analysis of ceramic breeder pebble beds under mechanical stresses. J. Nucl. Mater. **417**, 706–709 (2011). https://doi.org/10.1016/j.jnucmat.2010.12.131
19. S. Zhao, Y. Gan, M. Kamlah et al., Influence of plate material on the contact strength of Li_4SiO_4 pebbles in crush tests and evaluation of the contact strength in pebble-pebble contact. Eng. Fract. Mech. **100**, 28–37 (2013). https://doi.org/10.1016/j.engfracmech.2012.05.011
20. J.J. Lee, G.C. Park, K.Y. Kim et al., Numerical treatment of pebble contact in the flow and heat transfer analysis of a pebble bed reactor core. Nucl. Eng. Des. **237**, 2183–2196 (2007). https://doi.org/10.1016/j.nucengdes.2007.03.046
21. S. Wang, S. Wang, Q. Xu et al., Crushed model and uniaxial compression analysis of random packed ceramic pebble bed by DEM. Fusion Eng. Des. **128**, 53–57 (2018). https://doi.org/10.1016/j.fusengdes.2018.01.028
22. D.M. Kuang, J. Su, Z.R. Chen et al., Investigation of the size-dependent crushing behavior of Li_4SiO_4 pebbles via discrete element method. Fusion Eng. Des. **199**, 114105 (2024). https://doi.org/10.1016/j.fusengdes.2023.114105
23. J. Wang, M. Lei, H. Yang et al., Predicting the crushing behavior of pebbles: theoretical model and experiment verification. Fusion Eng. Des. **194**, 113929 (2023). https://doi.org/10.1016/j.fusengdes.2023.113929
24. Z.Y. Chen, G.Y. Li, K.M. Wei et al., Ultimate state and probability of particle breakage for rockfill materials based on fractal theory. Chin. J. Geotech. Eng. (in Chinese) **43**, 1192–1200 (2021). https://doi.org/10.11779/CJGE202107003
25. B. Zhao, J. Wang, M. Coop et al., An investigation of single sand particle fracture using X-ray micro-tomography. Géotechnique **65**, 625–641 (2015). https://doi.org/10.1680/geot.4.P.157
26. P. Wang, Z.Y. Yin, Z.Y. Wang, Micromechanical investigation of particle-size effect of granular materials in biaxial test with the role of particle breakage. J. Eng. Mech. **148**, 04021133 (2022). https://doi.org/10.1061/(ASCE)EM.1943-7889.0002039
27. Y. Xiao, M. Meng, A. Daouadji et al., Effects of particle size on crushing and deformation behaviors of rockfill materials. Geosci.

Front. **11**, 375–388 (2020). https://doi.org/10.1016/j.gsf.2018.10.010
28. L. Bao, J. Ma, W. Long et al., Fractal analysis in particle dissolution: a review. Rev. Chem. Eng. **30**, 261–287 (2014). https://doi.org/10.1515/revce-2013-0032
29. J. Ren, Z. Wang, B. Li et al., Fractal-time-dependent fick diffusion model of coal particles based on desorption-diffusion experiments. Energy Fuels **36**, 6198–6215 (2022). https://doi.org/10.1021/acs.energyfuels.2c00855
30. A. Nakata, M. Hyde, H. Hyodo et al., A probabilistic approach to sand particle crushing in the triaxial test. Géotechnique **49**, 567–583 (1999). https://doi.org/10.1680/geot.1999.49.5.567
31. S.A. Hall, M. Bornert, J. Desrues et al., Discrete and continuum analysis of localised deformation in sand using X-ray μCT and volumetric digital image correlation. Géotechnique **60**, 315–322 (2010). https://doi.org/10.1680/geot.2010.60.5.315
32. A. Hasan, K. Alshibli, Experimental assessment of 3D particle-to-particle interaction within sheared sand using synchrotron microtomography. Géotechnique **60**, 369–379 (2010). https://doi.org/10.1680/geot.2010.60.5.369
33. E. Andò, S.A. Hall, G. Viggiani et al., Grain-scale experimental investigation of localised deformation in sand: a discrete particle tracking approach. Acta Geotech. **7**, 1–13 (2012). https://doi.org/10.1007/s11440-011-0151-6
34. J. Fonseca, C. O'sullivan, M.R. Coop et al., Quantifying the evolution of soil fabric during shearing using directional parameters. Géotechnique **63**, 487–499 (2013). https://doi.org/10.1007/s11440-011-0151-6
35. S. Liu, J. Wang, C.Y. Kwok, Dem simulation of creep in one-dimensional compression of crushable sand. J. Geotech. Geoenviron. **145**, 04019060 (2019). https://doi.org/10.1061/(ASCE)GT.1943-5606.0002098
36. M. Lei, S. Xu, C. Guo et al., Design and thermal-hydraulic evaluation of helium-cooled ceramic breeder blanket for China fusion engineering test reactor. Int. J. Energ. Res. **42**, 1657–1663 (2018). https://doi.org/10.1002/er.3961

Authors and Affiliations

Jian Wang[1,2,3] · Ming-Zhun Lei[2] · Ming-Zong Liu[1] · Qi-Gang Wu[2,4] · Zi-Cong Cai[1] · Kai-Song Wang[1] · Hai-Shun Deng[1]

✉ Hai-Shun Deng
denghaishun@126.com

[1] Anhui University of Science and Technology, Huainan 232001, China

[2] Institute of Plasma Physics, Chinese Academy of Sciences, Hefei 230031, China

[3] The First Affiliated Hospital of Anhui University of Science and Technology (Huainan First People's Hospital), Huainan 232001, China

[4] University of Science and Technology of China, Hefei 230026, China